
BAYESIAN OPTIMIZATION FOR IDENTIFICATION OF OPTIMAL BIOLOGICAL DOSE COMBINATIONS IN PERSONALIZED DOSE-FINDING TRIALS

James Willard, Shirin Golchi, and Erica EM Moodie

Department of Epidemiology and Biostatistics

McGill University

Montreal, Canada

{james.willard}@mail.mcgill.ca

Abstract

Early phase, personalized dose-finding trials for combination therapies seek to identify patient-specific optimal biological dose (OBD) combinations, which are defined as safe dose combinations which maximize therapeutic benefit for a specific covariate pattern. Given the small sample sizes which are typical of these trials, it is challenging for traditional parametric approaches to identify OBD combinations across multiple dosing agents and covariate patterns. To address these challenges, we propose a Bayesian optimization approach to dose-finding which formally incorporates toxicity information into both the initial data collection process and the sequential search strategy. Independent Gaussian processes are used to model the efficacy and toxicity surfaces, and an acquisition function is utilized to define the dose-finding strategy and an early stopping rule. This work is motivated by a personalized-dose finding trial which considers a dual-agent therapy for obstructive sleep apnea, where OBD combinations are tailored to obstructive sleep apnea severity. To compare the performance of the personalized approach to a standard approach where covariate information is ignored, a simulation study is performed. We conclude that personalized dose-finding is essential in the presence of heterogeneity.

Keywords Bayesian adaptive clinical trial · constrained optimization · dose escalation · efficacy · Gaussian process · toxicity

1 Introduction

Early phase clinical trials assess the safety and efficacy of first-in human doses of experimental therapies. Bayesian adaptive designs, which utilize posterior or posterior predictive distributions for sequential decision making, are commonly employed for these trials, and can be divided into three major families: algorithmic, model-assisted, and model-based (Berry et al., 2010). Here, our focus is on model-based designs, which posit a full probability model for the dose-response surface of interest. Additionally, they permit clinicians to formally encode prior beliefs in the trial, which may be beneficial given the small sample sizes characteristic of early phase trials. Much of the historical work in early phase designs is motivated by the development of cytotoxic agents in oncology, where the goal is to find the maximum tolerated dose (MTD) while typically assuming monotonic dose-response surfaces and binary endpoints (O’Quigley et al., 1990; Babb et al., 1998).

Recently, interest has grown in molecularly targeted compounds which may display benefit at dosages lower than those that induce toxicity or the MTD (Le Tourneau et al., 2009). In these trials, traditional toxicity responses have been replaced by other drug-related biological effects, which are often measured on a continuous scale, e.g., plasma drug concentration and measures of target inhibition in tissues of interest (Korn, 2004; Le Tourneau et al., 2009). Additionally, many binary toxicity responses arise from dichotomizing a continuous measure, which is well known to lead to loss of information, decreased efficiency, increased sample sizes, and may introduce bias (Farewell et al., 2004; Royston et al., 2006; Wason et al., 2011). These developments have increased interest in continuous toxicity responses (e.g., Chen et al. (2010); Lee et al. (2012); Le-Rademacher et al. (2020)). Despite this, the literature for dose-finding using continuous responses remains less developed than that using binary responses. With the development of novel therapies where it is possible that the MTD is not the most efficacious dose, interest has grown in designs which incorporate both efficacy and toxicity information to find an optimal biological dose (OBD; e.g., Thall and Cook (2004); Yuan et al. (2016)). Furthermore, since monotonicity of the dose-response surfaces depends on the type of therapy being investigated and may not hold in

general (Li et al., 2017), flexible designs have been proposed to identify OBD combinations under non-monotonicity (e.g., Houede et al. (2010); Mozgunov and Jaki (2019b)) and for continuous dose-response surfaces (Mozgunov and Jaki, 2019a).

All dose-finding designs mentioned above assume the same dose is optimal for every patient in the population. We refer to this “one-size-fits-all” approach as *standard dose-finding*. With the continued identification and development of novel biomarkers, interest has grown in more personalized approaches to medicine. *Personalized dose-finding* seeks to find optimal doses based on individual patient characteristics. Despite this growing interest, the literature for personalized dose-finding trials remains underdeveloped as the limited sample sizes in these trials make it challenging to extend many parametric dose-finding methods to the personalized setting, where potentially many dose-covariate interaction terms must be estimated. Personalized dose-finding trials for monotherapy have been explored previously (e.g., Babb and Rogatko (2001); Guo and Zang (2022)). Our focus in this manuscript is on personalized dose-finding trials for combination therapies, where the additional dosing agents increase the dimensionality and exacerbate the estimation challenges. Mozgunov et al. (2022) investigated dual-agent personalized dose-finding with an application to an opiate detoxification trial, where the level of one of the agents was pre-specified externally by clinicians. Willard et al. (2023) proposed a flexible personalized dose-finding design for continuous responses which uses Bayesian optimization to explore all dosing dimensions under no monotonicity assumptions. However, they assumed a minimal toxicity setting where every dose combination was assumed to be safe, and so formal dose escalation rules were not considered. The present work extends this approach to the setting of higher-grade continuous toxicities by proposing a dose escalation scheme to collect the initial data, and by formally incorporating the toxicities into the search strategy employed by the Bayesian optimization based dose-finding method.

This work is motivated by a dose-finding design for a combination therapy which treats obstructive sleep apnea (OSA). OSA is a common sleep disorder which is estimated to affect over 930 million adults worldwide (Benjafield et al., 2019). Continuous positive airway pressure (CPAP) is the standard treatment since it is very effective, but it is often poorly tolerated and results in

low patient adherence (Rotenberg et al., 2016). There is currently no approved pharmacotherapy for OSA, though several recent studies have investigated the combination of antimuscarinic agents (oxybutynin and aroxybutynin) and a norepinephrine reuptake inhibitor (atomoxetine) as therapy (Schweitzer et al., 2023; Aishah et al., 2023; Rosenberg et al., 2022). While these studies suggest that combination therapy is effective in reducing a key continuous endpoint, they revealed that potential response heterogeneity exists with respect to OSA severity and so a more targeted therapeutic approach would be beneficial. The current work aims to develop a design that can identify OBD combinations which are tailored to OSA severity.

The remainder of this manuscript is organized in the following manner. We first provide a brief introduction to Bayesian optimization and review the dose-finding approaches established for continuous responses in Willard et al. (2023). Next, we propose a formal dose-escalation scheme for continuous toxicities, which generalizes these approaches to the setting of higher-grade toxicities. This is followed by a simulation study where we compare the performance of the proposed approaches under two scenarios. We then consider the previously described dose-finding design for a dual-agent therapy to treat OSA. We conclude with a discussion.

2 Bayesian Optimization for Dose-Finding

Personalized Dose-Finding Consider a set of P discrete covariates $\mathbf{Z} = \{Z_p\}_{p=1}^P$, and define K strata as the Cartesian product of their levels. Personalized dose finding seeks to identify optimal dose combinations for each of the K strata. We refer to the continuous therapeutic function of interest (i.e., efficacy or utility) as the *efficacy* function, denoted by $f(\mathbf{d}, \mathbf{z})$, and define the continuous toxicity function as $g(\mathbf{d}, \mathbf{z})$, where both are assumed to have been transformed such that smaller values denote being more desirable. Our goal is to find, for each stratum k , the combination of J dosing agents $\mathbf{d} = (d_1, \dots, d_J) \in \mathbb{D} \subset \mathbb{R}^J$ which minimizes $f(\mathbf{d}, \mathbf{z}_k)$, subject to a tolerable level of toxicity g_k^\dagger :

$$\underset{\mathbf{d} \in \mathbb{D}}{\operatorname{argmin}} f(\mathbf{d}, \mathbf{z}_k) \quad \text{subject to} \quad g(\mathbf{d}, \mathbf{z}_k) \leq g_k^\dagger \quad \text{for } k = 1, \dots, K.$$

Unique toxicity thresholds g_k^\dagger allow permissible toxicity to be defined with respect to specific covariate profiles. This is useful in settings where higher levels of toxicity may be permitted for more severe disease subtypes, for example. We solve the above minimization problem using Bayesian optimization, a derivative-free method which finds the global optima of expensive-to-evaluate objective functions (Garnett, 2023). Bayesian optimization relies on stochastic surrogate models, commonly Gaussian Processes (GP), to estimate the efficacy and toxicity functions, and then employs an acquisition function to define a sequential search policy. It has been historically used for global optimization problems within the engineering, machine learning, and computer experiments literature (e.g., Kushner (1964); Zhilinskas (1975); Jones et al. (1998); Gramacy (2020)), and has seen recent application in early phase dose-finding trials (Takahashi and Suzuki, 2021b,a; Willard et al., 2023). Below, we generalize the approach proposed in Willard et al. (2023) to higher-grade toxicity settings, by using Bayesian optimization for dose-finding in the presence of toxicity constraints.

To start, $n = \sum_{k=1}^K r_k \times c_k$ initial responses are collected, where for the k^{th} stratum, r_k independent patients are evaluated at c_k initial dose combinations. A proposed method for collecting these initial responses under uncertain toxicity is described in detail further below. These initial responses yield noisy observations of both the efficacy function, $y_f = f(\mathbf{d}, \mathbf{z}) + \epsilon_f$, and the toxicity function, $y_g = g(\mathbf{d}, \mathbf{z}) + \epsilon_g$, where $\epsilon_f \sim N(0, \sigma_{y_f}^2)$, $\epsilon_g \sim N(0, \sigma_{y_g}^2)$, and $\mathbf{y} = (y_f, y_g)$. In many contexts, it is reasonable to assume conditional independence between the efficacy and toxicity functions given dose, and so we do throughout. We describe how to relax this assumption in the discussion section for scenarios where they are expected to remain correlated after adjusting for dose. Independent GP priors are placed on the efficacy and toxicity functions, the details of which are described below for the efficacy function only since those for toxicity are similar. In cases where it is reasonable to assume the dose-toxicity function is monotonically non-decreasing, GP models incorporating monotonicity constraints (Lin and Dunson, 2014; Golchi et al., 2015) or less flexible models could be utilized, though we do not consider these approaches here. The dose-toxicity function may be non-monotonic in cases where a toxicity score is defined as an aggregate of adverse events (AEs;

e.g., Le-Rademacher et al. (2020)), where different dose combinations yield different distributions of the individual AEs that, when aggregated, potentially yield a non-monotonic dose-toxicity surface. We utilize the following unconstrained GP model for the efficacy function:

$$f(\mathbf{d}, \mathbf{z}) \sim GP(m_f(\mathbf{d}, \mathbf{z}), \nu_f \mathcal{K}_f((\mathbf{d}, \mathbf{z}), (\mathbf{d}', \mathbf{z}')))$$

where $m_f(\mathbf{d}, \mathbf{z})$ is the mean function, and $\mathcal{K}_f((\mathbf{d}, \mathbf{z}), (\mathbf{d}', \mathbf{z}'))$ is a correlation function (kernel) multiplied by scale parameter ν_f (Binois and Gramacy, 2021). The scale parameter determines the variability of the efficacy function throughout the dose combination space. We utilize GP models with a constant mean function, $m_f(\mathbf{d}, \mathbf{z}) = \beta_f$, though note that additional information about the efficacy function (e.g., pharmacokinetic/pharmacodynamic models) or toxicity function (e.g., quantitative systems toxicology models) can be incorporated into the mean function. We employ a stationary anisotropic squared exponential kernel,

$$\mathcal{K}_f((\mathbf{d}, \mathbf{z}), (\mathbf{d}', \mathbf{z}')) = \exp \left\{ - \left(\sum_{j=1}^J \frac{(d_j - d'_j)^2}{2l_{f,j}^2} + \sum_{p=1}^P \frac{(z_p - z'_p)^2}{2l_{f,p}^2} \right) \right\} \quad (1)$$

parameterized by characteristic length-scales $\{l_{f,1}, \dots, l_{f,P}\}$. These control how quickly the correlation between two dose combinations decays with respect to each dosing agent and across covariate patterns. Throughout this work, we assume stationary dose-response surfaces, where the degree of correlation between two dose combinations depends only on their distance from one another in the input space. We comment on relaxing this assumption in the discussion.

Specifying this GP prior induces a multivariate normal distribution on the efficacy function observations, $\mathbf{y}_f \sim N(\beta_f \mathbf{1}_n, \nu_f \mathbf{K}_f)$, where $\mathbf{K}_f(i, j) = \mathcal{K}_f((\mathbf{d}_i, \mathbf{z}_i), (\mathbf{d}_j, \mathbf{z}_j)) + \tau_f^2 \mathbf{1}_{i=j}$ and τ_f^2 is a noise parameter. After data $\mathcal{D} = \{(\mathbf{d}_i, \mathbf{z}_i, \mathbf{y}_i)\}_{i=1}^n$ are observed, the kernel hyperparameters $\boldsymbol{\theta} = \{\nu_f, \tau_f^2, l_{f,1}, \dots, l_{f,P}\}$ are estimated via maximum likelihood and replaced by their point estimates, taking an empirical Bayes approach (Binois and Gramacy, 2021).

This yields the posterior distribution of the efficacy function at a new dose combination $\tilde{\mathbf{d}}$ in stratum k , denoted by $\tilde{\mathbf{d}}_k = (\tilde{\mathbf{d}}, \tilde{\mathbf{z}}_k)$, as $p(f \mid \mathcal{D}, \tilde{\mathbf{d}}_k) = N(\mu_f(\tilde{\mathbf{d}}_k), \sigma_f^2(\tilde{\mathbf{d}}_k))$ (Binois and Gramacy, 2021),

such that

$$\begin{aligned}
\mu_f(\tilde{\mathbf{d}}_k) &= \hat{\beta}_f + \mathbf{k}_f(\tilde{\mathbf{d}}_k)^T \mathbf{K}_f^{-1} (\mathbf{y}_f - \hat{\beta}_f \mathbf{1}) \\
\sigma_f^2(\tilde{\mathbf{d}}_k) &= \nu_f \mathcal{K}_f(\tilde{\mathbf{d}}_k, \tilde{\mathbf{d}}_k) - \nu_f \mathbf{k}_f(\tilde{\mathbf{d}}_k)^T \mathbf{K}_f^{-1} \mathbf{k}_f(\tilde{\mathbf{d}}_k) + \frac{(1 - \mathbf{k}_f(\tilde{\mathbf{d}}_k)^T \mathbf{K}_f^{-1} \mathbf{1})^2}{\mathbf{1}^T \mathbf{K}_f^{-1} \mathbf{1}} \\
\hat{\beta}_f &= \frac{\mathbf{1}^T \mathbf{K}_f^{-1} \mathbf{y}_f}{\mathbf{1}^T \mathbf{K}_f^{-1} \mathbf{1}}
\end{aligned} \tag{2}$$

where \mathbf{K}_f is $n \times n$ and $\mathbf{k}_f(\tilde{\mathbf{d}}_k) = [\mathcal{K}_f((\mathbf{d}_1, \mathbf{z}_1), \tilde{\mathbf{d}}_k), \dots, \mathcal{K}_f((\mathbf{d}_n, \mathbf{z}_n), \tilde{\mathbf{d}}_k)]^T$ is $n \times 1$. The posterior distribution of the toxicity function at $\tilde{\mathbf{d}}$ within stratum k is obtained similarly and has the same functional form as above but where f is replaced by g for all observations and kernel hyperparameters.

The next dose combination $\mathbf{d}_k^{(c_k+1)}$ within stratum k , is then selected as that which maximizes an acquisition function, denoted by $\alpha(\tilde{\mathbf{d}}_k \mid \mathcal{D})$:

$$\mathbf{d}_k^{(c_k+1)} = \underset{\tilde{\mathbf{d}} \in \mathbb{D}}{\operatorname{argmax}} \alpha(\tilde{\mathbf{d}}_k \mid \mathcal{D}).$$

One possible acquisition function which can be used in the presence of toxicity constraints is a constrained version of the Expected Improvement (cEI), defined as

$$\alpha_{cEI}(\tilde{\mathbf{d}}_k \mid \mathcal{D}) = \mathbb{E} \left[\max(0, f_k^* - f(\tilde{\mathbf{d}}_k)) \mathbb{1}\{g(\tilde{\mathbf{d}}_k) \leq g_k^\dagger\} \mid \mathcal{D}, \tilde{\mathbf{d}}_k \right],$$

and available in closed form under the assumption of conditional independence between the efficacy and toxicity functions given dose (Jones et al., 1998; Gardner et al., 2014):

$$\alpha_{cEI}(\tilde{\mathbf{d}}_k \mid \mathcal{D}) = \left[(f_k^* - \mu_f(\tilde{\mathbf{d}}_k)) \Phi \left(\frac{f_k^* - \mu_f(\tilde{\mathbf{d}}_k)}{\sigma_f(\tilde{\mathbf{d}}_k)} \right) + \sigma_f(\tilde{\mathbf{d}}_k) \phi \left(\frac{f_k^* - \mu_f(\tilde{\mathbf{d}}_k)}{\sigma_f(\tilde{\mathbf{d}}_k)} \right) \right] \Phi \left(\frac{g_k^\dagger - \mu_g(\tilde{\mathbf{d}}_k)}{\sigma_g(\tilde{\mathbf{d}}_k)} \right).$$

Above, f_k^* denotes the current optimum of the efficacy function in stratum k , g_k^\dagger denotes the stratum-specific toxicity constraint, $\Phi(\cdot)$ and $\phi(\cdot)$ denote the standard normal cumulative distribution function and probability density function, respectively, and $\mu(\tilde{\mathbf{d}}_k)$ and $\sigma(\tilde{\mathbf{d}}_k)$ are given above in (2).

The expression inside the brackets serves to balance the tradeoff between exploring regions of the dose combination space where the efficacy function is imprecisely estimated, and exploiting regions which have desirable values of the efficacy function. This trade-off is weighted by the posterior probability of satisfying the toxicity constraint, giving higher weight to points which are

more likely to be safe. Under a noisy setting, we set $f_k^* = \min_{\tilde{\mathbf{d}} \in \mathbb{A}_k} \boldsymbol{\mu}_f(\tilde{\mathbf{d}}_k)$, the minimum of the posterior mean of the efficacy function in the set of safe doses, \mathbb{A}_k , in stratum k . A dose combination is considered to be safe if $P(g(\tilde{\mathbf{d}}_k) \leq g_k^\dagger \mid \mathcal{D}) > \gamma_k$, where γ_k is a tuning parameter which can be specified through a sensitivity analysis. Larger values of γ_k imply a more stringent definition of safety whereas smaller values imply a more permissive definition. In the event where $\mathbb{A}_k = \emptyset$ during a single iteration, f_k^* is set as the posterior mean of the maximizer of this probability statement (i.e., the average efficacy at the dose predicted to be safest; Gelbart et al. (2014)). We note that dose-finding in stratum k terminates before assigning $\mathbf{d}_k^{(c_k+1)}$ if no dose combinations are predicted to be safe for several consecutive iterations. Since observations of the toxicity function are noisy, random variation in the data may cause incorrect early stopping if it is permitted after only a single violation of this probability statement. Thus, we require the probability statement to be violated for $J + 1$ iterations before termination, where J is the number of dosing agents, following a recommendation for stopping rules under noise (Huang et al., 2006).

After observing responses for r_k new patients at $\mathbf{d}_k^{(c_k+1)}$, the data are updated and the GP models are refit to obtain new posterior distributions for f and g . Then $s = 1, \dots, S$ samples $f^{(s)}(\tilde{\mathbf{d}}_k)$ and $g^{(s)}(\tilde{\mathbf{d}}_k)$ from these posteriors are obtained to yield S samples from the posterior of the optimal dose combination $p(\mathbf{d}_{opt,k} \mid \mathcal{D})$ as:

$$\mathbf{d}_{opt,k}^{(s)} = \underset{\tilde{\mathbf{d}} \in \mathbb{A}_k^{(s)}}{\operatorname{argmin}} f^{(s)}(\tilde{\mathbf{d}}_k)$$

where the admissible set of safe doses in stratum k is defined as $\mathbb{A}_k^{(s)} = \{\tilde{\mathbf{d}} : P(g^{(s)}(\tilde{\mathbf{d}}_k) \leq g_k^\dagger) > \gamma_k\}$. Dose-finding within each stratum continues until the sample size limit is reached or a stratum-specific early stopping rule is satisfied. We permit early stopping in stratum k when $\max_{\tilde{\mathbf{d}} \in \mathbb{D}} \alpha_{cEI}(\tilde{\mathbf{d}}_k \mid \mathcal{D}) < \delta_k$. Due to random variability in the data, we require this statement to be satisfied for at least $(J + 1)$ consecutive iterations, where δ_k is calibrated through sensitivity analysis. For example, early stopping would occur at iteration 7 if $\delta_k = 0.11$ and $\max_{\tilde{\mathbf{d}} \in \mathbb{D}} \alpha_{cEI}(\tilde{\mathbf{d}}_k \mid \mathcal{D})$ is 0.12, 0.10, 0.09, 0.08 for iterations 4, 5, 6, 7, respectively. For convenience below, we refer to this as early stopping for “efficacy”, noting that it is technically early stopping due to minimal expected

improvement over the current best observation, which need not imply a significant therapeutic response. The sequential procedure described above is referred to as the *personalized optimization algorithm*. Note that in the present work and in contrast to the personalized optimization algorithm in Willard et al. (2023), we explicitly model toxicity and incorporate it into the sequential search policy defined by $\alpha_{cEI}(\tilde{\mathbf{d}}_k \mid \mathcal{D})$. We note that the *standard optimization algorithm* is a special case of the personalized approach, where covariate information is ignored (i.e., $\mathbf{Z} = \emptyset$) and only the dosing agents themselves are considered for optimization.

3 Initial Data Collection

Expansion of Dose Combination Region It is important to limit to the extent possible the number of patients who experience adverse events and who are assigned to toxic doses. After the initial data are collected and the dose-finding algorithm described above begins, the achievement of these objectives is controlled through the cEI acquisition function, which gives lower values to doses which are predicted to be toxic, making them less likely to be evaluated. To limit toxicities among the initial patients, however, doses must be explored in a sequential manner, where lower (i.e., less toxic) doses are evaluated before higher (i.e., more toxic) doses. In a monotherapy setting, this is straightforward since there is a natural ordering from lower to higher doses. In a combination therapy setting, this is more challenging since many dose combinations may yield comparable toxicity and so there is no longer a natural ordering. One challenge in designing a dose-escalation scheme under this setting is in deciding which doses should be candidates for evaluation at each stage of the escalation. For dual-agent combination therapies, Sweeting and Mander (2012) showed that the MTD was more efficiently identified when, at each iteration of the dose escalation algorithm, the levels of all dosing agents were permitted to be increased rather than the level of a single agent only. This amounts to allowing dose escalation to proceed along the “diagonal” when considering a two-dimensional dosing grid. We adopt a similar idea below by permitting our continuous dose combination region of interest in stratum k , denoted by \mathbb{D}_k , to be expanded in all coordinate directions at each iteration of dose escalation. We note that expansion of \mathbb{D}_k does not control which doses within this region will be evaluated. That choice is controlled separately using the cEI ac-

quisition function as previously described. However, \mathbb{D}_k serves to restrict the choice of doses the cEI may consider at each iteration, thereby ensuring the initial doses are explored in an escalating fashion.

Consider a continuous dose combination region within stratum k , which we assume to be standardized and bounded, $\mathbb{D}_k \subseteq [0, 1]^J$. At the beginning of the dose escalation scheme, we define \mathbb{D}_k to be the lowest standardized dose only, denoted by $\mathbf{d}_k^{(0)} = \mathbf{0}$. We start by evaluating this dose, after which \mathbb{D}_k is expanded. At each iteration of the dose escalation scheme, the sequentially expanded \mathbb{D}_k takes the form of a lower half-space intersected with $[0, 1]^J$. To define this intersection, we select a value ρ_k which represents the maximum amount by which a single coordinate dosing dimension may be increased. Then at iteration q , we set $\mathbb{D}_k^{(q)} = \{\mathbf{d} \in [0, 1]^J : \mathbf{w}_k^T \mathbf{d} \leq \rho_k \times q, \mathbf{w}_k = \mathbf{1}_J\}$. Smaller values of ρ_k imply a slower expansion of \mathbb{D}_k whereas larger values imply a faster expansion of \mathbb{D}_k . This rate of expansion should depend on the potential severity of toxicities considered, with slower expansion being necessary for contexts which are expected to contain more severe toxicities. We choose \mathbf{w}_k to be the J -dimensional vector of ones to perform uniform expansion across all dosing dimensions. This could be relaxed if prior information suggests non-uniform expansion should be permitted, e.g., if one dosing agent is known to be much safer than the others. We note that expansion of \mathbb{D}_k will continue to eventually include the entire unit hypercube, even if there are regions which are predicted to be overly toxic. Expansion is permitted because exploration within the space is controlled by the cEI acquisition function, which avoids toxic regions and will terminate the dose-finding algorithm in the event of there being no safe doses. As mentioned above, the expansion of \mathbb{D}_k serves only to restrict which doses the cEI can explore at each iteration, ensuring doses are evaluated in an escalating manner.

As an example of this sequential expansion of \mathbb{D}_k , consider a dual-agent dose combination setting with standardized doses in $[0, 1]^2$ and where $\mathbf{d}^{(0)} = (0, 0)$ and $\rho_k = 0.25$. After evaluating $\mathbf{d}_k^{(0)}$, we consider the first iteration of expansion and set $q = 1$. Then we define $\mathbb{D}_k^{(1)} = \{\mathbf{d} \in [0, 1]^J : \mathbf{w}_k^T \mathbf{d} \leq 0.25, \mathbf{w}_k = \mathbf{1}_J\}$. That is, at the first iteration, \mathbb{D}_k becomes the triangle defined by vertices $\{(0, 0), (0, 0.25), (0.25, 0)\}$ from which the cEI determines $\mathbf{d}^{(1)}$. At the second iteration of expansion

sion, we set $q = 2$ and define $\mathbb{D}_k^{(2)} = \{\mathbf{d} \in [0, 1]^J : \mathbf{w}_k^T \mathbf{d} \leq 0.5, \mathbf{w}_k = \mathbf{1}_J\}$. Thus, at the second iteration, \mathbb{D}_k becomes the triangle defined by vertices $\{(0, 0), (0, 0.5), (0.5, 0)\}$ from which the cEI determines $\mathbf{d}^{(2)}$. This expansion continues until \mathbb{D}_k is defined as the entire unit hypercube, or until the dose-finding algorithm terminates.

To further promote exploration of the dose combination region during the expansion of \mathbb{D}_k , regions which are close to previously evaluated doses may be removed. That is, until $\mathbb{D}_k = [0, 1]^J$, a modified region can be defined at each iteration as $\mathbb{D}_k^{(q)*} = \mathbb{D}_k^{(q)} \setminus \mathbb{C}_k^{(q)}$, where $\mathbb{C}_k^{(q)} = \bigcup_{i=0}^{q-1} \mathcal{N}_k^{(i)}$ is the set of regions or neighbourhoods $\mathcal{N}_k^{(i)}$ (e.g., hypercubes defined by a small side length l_k , where $l_k \ll \rho_k$) which surround the previously evaluated dose combinations $\{\mathbf{d}_k^{(i)}\}_{i=0}^{q-1}$. Using $\mathbb{D}_k^{(q)*}$ instead of $\mathbb{D}_k^{(q)}$ promotes exploration of the input space during the initial stages of dose-finding, and may prevent the algorithm from getting stuck in certain regions. This can lead to improved GP model fits at early iterations which may improve algorithm performance overall.

4 Simulation Study

In this section, we perform a simulation study to compare the performance of the personalized and standard approaches for a dual-agent (i.e., $J = 2$) therapy under two scenarios which consider a single binary covariate Z_1 . The first scenario considers no response heterogeneity across the strata with respect to the objective and toxicity surfaces, whereas the second considers response heterogeneity with respect to both surfaces. The scenarios do not permit early stopping for efficacy (i.e., $\delta_k = 0$ in the stopping rule), which is investigated in the next section. Early stopping for toxicity is still permitted, however, where we stop for toxicity in stratum k if $P(g(\tilde{\mathbf{d}}) \leq g_k^\dagger \mid \mathcal{D}) < 0.9 \forall \tilde{\mathbf{d}}$ is satisfied $J+1 = 3$ consecutive times. In this event, the personalized algorithm permits dose-finding to continue in the other stratum unless it has also stopped for toxicity. We use values of Z_1 to index the true optimal dose combinations, $\mathbf{d}_{opt,k}$, and the values of the objective and toxicity functions at the $\mathbf{d}_{opt,k}$, denoted by $f_{opt,k}$ and $g_{opt,k}$, respectively. To make the simulations more computationally feasible, we modify the algorithms to return a point estimate $\hat{\mathbf{d}}_{opt,k} = \operatorname{argmin}_{\tilde{\mathbf{d}} \in \mathbb{A}_k} \mu(\tilde{\mathbf{d}}, \tilde{\mathbf{z}}_k)$ rather than the entire posterior distribution of $\mathbf{d}_{opt,k}$. Performance is compared for two values of

the toxicity threshold $g_k^\dagger \in \{0.2, 0.5\}$ to assess how the distance of the $\mathbf{d}_{opt,k}$ from the g_k^\dagger contour impacts the optimization. We do not consider a scenario where all dose combinations are toxic, since the dose ranges investigated in combination therapies are expected to be better targeted due to the previous early phase studies of each individual agent (Sweeting and Mander, 2012).

We utilize standardized dose combinations $\mathbf{d} = (d_1, d_2) \in [0, 1]^2$ which are separated in each coordinate direction by 0.25 units, creating a grid of 25 potential dose combinations in total. While the proposed method can optimize over the continuous dose combination space, engineering constraints may restrict the precision to which an agent can be manufactured. Thus, any constraints should be incorporated into the optimization, as we have done here. We set the point estimate of the recommended dose, $\hat{\mathbf{d}}_{opt,k}$, as $\operatorname{argmin}_{\tilde{\mathbf{d}} \in \mathbb{A}_k} \mu(\tilde{\mathbf{d}}, \tilde{\mathbf{z}}_k)$ and the next dose combination to be evaluated, $\mathbf{d}^{(c_k+1)}$, as the maximizer of $\alpha_{cEI}(\tilde{\mathbf{d}} \mid \mathcal{D}, \tilde{\mathbf{z}}_k)$. For the initial data collection, we set $\rho_k = 0.25$ and utilize the modified $\mathbb{D}_k^{(q)*}$ to promote exploration at the earlier iterations of the algorithm. We define $\mathbb{D}_k^{(q)*}$ by setting $\mathbb{C}_k^{(q)} = \{\mathbf{d}_k^{(i)}\}_{i=0}^{q-1}$. Doing so prevents any previously evaluated dose combination from being selected as the next dose until after iteration $q = 8$, which is the iteration at which \mathbb{D}_k becomes the unit hypercube. At each evaluated dose combination, the personalized algorithm uses $r_k = 2$ participants and the standard algorithm uses $r_k = 4$ participants. This ensures that both algorithms use the same number of total participants at each iteration, where the maximum sample size is set to be 80 participants.

We define $f(\mathbf{d}, z_1)$ and $g(\mathbf{d}, z_1)$ to be the continuous objective and toxicity surfaces which are defined using the multivariate normal density $h(\boldsymbol{\mu}) = N(\boldsymbol{\mu}, \boldsymbol{\Sigma})$ with the same covariance matrix $\boldsymbol{\Sigma} = \begin{bmatrix} 0.1 & 0 \\ 0 & 0.1 \end{bmatrix}$ but with different mean vectors: $\boldsymbol{\mu}_1 = (0.5, 0.5)^T$, $\boldsymbol{\mu}_2 = (1, 1)^T$, $\boldsymbol{\mu}_3 = (0.25, 0.75)^T$, $\boldsymbol{\mu}_4 = (0.75, 0.25)^T$, $\boldsymbol{\mu}_5 = (0.75, 1.25)^T$, and $\boldsymbol{\mu}_6 = (1.25, 0.75)^T$. For each scenario, the data generating mechanism is $y_f = f(\mathbf{d}, z_1) + \epsilon_f$ and $y_g = g(\mathbf{d}, z_1) + \epsilon_g$ where $\epsilon_f \sim N(0, \sigma_{y_f}^2)$ and $\epsilon_g \sim N(0, \sigma_{y_g}^2)$. The specifications of $f(\mathbf{d}, z_1)$ and $g(\mathbf{d}, z_1)$ are included in Table 1 (rows labeled ‘‘Simulation Study’’) and are plotted in panel A of Figures 1 and 2. The values of σ_{y_f} and σ_{y_g} are chosen to ensure specific standardized effect sizes (ses) at the optimal dose combination, defined as $ses_f = |f_{opt}|/\sigma_{y_f}$ and $ses_g = |g_{opt}|/\sigma_{y_g}$. Willard et al. (2023) considered several values for

ses_f , which were 0.79/1/3.77 and represented the 25th/50th/75th percentiles of ses from a meta-analysis of dose-responses for a large drug development portfolio at a pharmaceutical company (Thomas et al., 2014), and showed that a larger ses led to better performance of the algorithms. As we expect these results to generalize to the current setting, we focus specifically on $ses_f = ses_g = 1$, which represents the median ses we might expect for a new combination therapy. All computing is performed in R (R Core Team, 2022). The efficacy and toxicity functions are modeled using constant mean GP models with the anisotropic squared exponential kernel previously described. An empirical Bayes approach is adopted toward the GP hyperparameters (Binois and Gramacy, 2021), where initial values are utilized until convergence of the maximum likelihood estimation, which typically occurs within the first few iterations. For the lengthscale parameters, these values are $\sqrt{J + P}/2$, which is the midpoint of the maximal distance between two points on the unit cube defined by standardizing J dosing agents and P covariates. For the noise parameters, these values are the observed sample variances $\hat{\sigma}_f^2$ and $\hat{\sigma}_g^2$ for the objective and toxicity function models, respectively.

Three criteria are used to quantify algorithm performance and are estimated using $m = 1, \dots, 1000$ Monte Carlo simulations. The expected number of toxic dose combinations administered to n_k participants is defined as follows:

$$E_{y|z_k}[\text{toxic doses}] \approx \frac{1}{1000} \sum_{m=1}^{1000} \left[\sum_{i=1}^{n_k} \mathbb{1} \left\{ g(\mathbf{d}_i^{(m)}, z_k) > g_k^\dagger \right\} \right]. \quad (3)$$

To assess how close $\hat{\mathbf{d}}_k$ is to $\mathbf{d}_{opt,k}$ at each iteration, the expected number of dosing units is defined as their Euclidean distance divided by the distance between each dose combination, which is 0.25 in the simulations:

$$E_{y|z_k}[\text{dose units}] \approx \frac{1}{1000} \sum_{m=1}^{1000} \frac{\sqrt{(\hat{d}_1^{(m)} - d_{1,opt})_k^2 + (\hat{d}_2^{(m)} - d_{2,opt})_k^2}}{0.25}. \quad (4)$$

To assess how well the pointwise posterior distribution of the objective function at $\hat{\mathbf{d}}_k$ estimates the true value $f_{opt,k}$, we use the expected root posterior squared error loss (RPSEL) which is estimated

using $s = 1, \dots, 10000$ posterior samples $f^{(s)}(\hat{\mathbf{d}}_k, z_k)$:

$$E_{y|z_k}[RPSEL] \approx \frac{1}{1000} \sum_{m=1}^{1000} \left[\frac{1}{10000} \sum_{s=1}^{10000} (f^{(s)}(\hat{\mathbf{d}}_k^{(m)}, z_k) - f_{opt,k})^2 \right]^{\frac{1}{2}}. \quad (5)$$

Panels B-D of Figures 1 and 2 plot these criteria by iteration, showcasing the performance of the algorithms throughout the optimization process.

Scenario 1 considers the case of no response heterogeneity. Under this scenario, the personalized and standard algorithms administer a comparable number of toxic doses, where the number is higher when $\mathbf{d}_{opt,k}$ is closer to the tolerable toxicity contour g_k^\dagger (Panel B of Figure 1). Under the more stringent toxicity threshold $g_k^\dagger = 0.2$, the personalized algorithm incorrectly stopped for toxicity in both strata 0.1% of the time, whereas the standard algorithm incorrectly stopped 0.3% of the time (results not shown). Neither algorithm incorrectly stopped under the more permissible toxicity threshold. A separate series of simulations was performed which did not perform dose escalation for the initial doses, but rather randomly selected the same number of initial doses as in the simulations described above (results not shown). Under this setting, the expected number of toxic doses administered was 11.9/11.9 for $g_k^\dagger = 0.2$ under the personalized/standard algorithm and 5.3/5.24 for $g_k^\dagger = 0.5$ under the personalized/standard algorithm. Thus, utilizing a dose escalation scheme results in a decrease in the number of toxic doses administered of roughly 66% and 74% for $g_k^\dagger = 0.2$ and $g_k^\dagger = 0.5$, respectively, underscoring the importance of dose escalation under higher-grade toxicity settings. Both the personalized and standard algorithms converge to the $\mathbf{d}_{opt,k}$, with the optimization being more efficient when $\mathbf{d}_{opt,k}$ is further from the permissible toxicity contour (i.e., $g_k^\dagger = 0.5$ vs $g_k^\dagger = 0.2$ in Panel C of Figure 1). Additionally, they each yield a posterior distribution which estimates the $f_{opt,k}$ comparably (Panel D of Figure 1). The sudden drop in RPSEL after iteration 8 results from the dose escalation scheme ending. This permits the algorithms to explore any dose in the dose combination region which leads to improved optimization. Overall, both algorithms yield acceptable performance under no response heterogeneity, though, as expected, the standard algorithm is slightly more efficient.

Scenario 2 considers the case of response heterogeneity with respect to both the efficacy and toxicity surfaces. As in the previous scenario, the personalized and standard algorithms administer a comparable number of toxic doses, where the number is higher when $\mathbf{d}_{opt,k}$ is closer to the tolerable toxicity contour g_k^\dagger (Panel B of Figure 2). Under the more stringent toxicity threshold $g_k^\dagger = 0.2$, the personalized algorithm incorrectly stopped for toxicity in both strata 0.1% of the time, whereas the standard algorithm incorrectly stopped more frequently at 1% of the time (results not shown). This difference results from the personalized algorithm permitting stratum-specific early stopping for toxicity, where the second stratum continues to be explored in the event of the first being stopped. Neither algorithm incorrectly stopped under the more permissible toxicity threshold. The personalized algorithm converges to the $\mathbf{d}_{opt,k}$, with the optimization being more efficient when $\mathbf{d}_{opt,k}$ is further from the permissible toxicity level (Panel C of Figure 1). However, the standard algorithm does not converge to $\mathbf{d}_{opt,k}$. As discussed in Willard et al. (2023), the marginal response surfaces are bimodal mixture distributions whose components consist of the equally weighted strata. Even though its use of the cEI may promote exploration of both modes during optimization, the standard algorithm still cannot determine how to optimally assign doses with respect to Z_1 , a major disadvantage as compared to the personalized approach. Finally, the personalized algorithm yields posterior distributions which estimate the $f_{opt,k}$ well (Panel D of Figure 2), whereas the standard algorithm does not. Overall, the personalized algorithm is capable of handling response heterogeneity with respect to the efficacy and toxicity surfaces, while the standard algorithm cannot.

5 Dose-Finding Design for Obstructive Sleep Apnea Therapy

Obstructive sleep apnea (OSA) is a common sleep disorder which affects over 930 million adults worldwide (Benjafield et al., 2019) and for which no pharmacotherapy has been approved. One continuous measure used to quantify OSA severity is the apnea-hypopnea index with 4% oxygen desaturation (AHI_4), which is measured in the number of apnea/hypopnea events per hour. Mild to moderate OSA is defined as 10-30 events per hour, and severe OSA is defined as 30 or more events per hour (Schweitzer et al., 2023). Based on a recently improved understanding of OSA’s pathophysiology, several studies have proposed a combination of one of two antimuscarinic agents (oxy-

butynin and aroxybutynin) and a single norepinephrine reuptake inhibitor (atomoxetine) to serve as a potential pharmacotherapy (Schweitzer et al., 2023; Aishah et al., 2023; Rosenberg et al., 2022). These studies assessed several combinations of the dosing agents on the reduction in AHI_4 from baseline. The evaluation times ranged from a single night up to four weeks on treatment, and concluded that the proposed drug combinations display potential as a therapy for OSA. Furthermore, it was noted that a targeted therapeutic approach might prove beneficial in future studies to handle possible response heterogeneity (Aishah et al., 2023). The dose-finding design proposed below is inspired by findings from Schweitzer et al. (2023), which investigated the combination of aroxybutynin (0/2.5/5 mg) and atomoxetine (75 mg). While results were not analyzed separately by OSA severity subtype, Figure 2 of Schweitzer et al. (2023) suggests there is potential response heterogeneity with respect to these subtypes. For the mild to moderate subtype, the combinations (aroxybutynin/atomoxetine) 2.5mg/75mg and 5mg/75mg seem to yield a similar reduction in AHI_4 , whereas for the severe subtype, the reduction under 5mg/75mg may be greater. However, it was observed that a larger number of AEs resulted from the 5mg/75mg combination, though none were serious. To achieve maximal reduction in AHI_4 in the severe subtype, we may be willing to tolerate a larger number of AEs than for the mild to moderate subtype. In this case, the OBD combination would be 2.5mg/75mg for the mild to moderate subtype, but would be the 5mg/75mg combination for the severe subtype. Considering the above, we propose a personalized dose-finding design which tailors the OBD combination to OSA subtype and which permits different toxicity thresholds g_k^\dagger for the severe versus mild to moderate subtypes.

To quantify the overall impact of AEs at each dose combination, we follow the approach in Le-Rademacher et al. (2020), who define a non-negative AE burden score that considers both the frequency and severity of the adverse events. Schweitzer et al. (2023) report the frequency of the most commonly occurring AEs; unfortunately, the grade (severity) information was not provided. However, since no severe adverse events were reported, we define the score by restricting our focus to grades 1-3 only, which we assume to occur 10%/45%/45% of the time independent of the type of AE, reflecting the belief that patients are more likely to remember and report higher graded

events. Let Y_{icg} be the indicator that the i^{th} patient experiences an AE of type c which is of grade g , where $g = 1, 2, 3$ and where $c = 1, \dots, 8$ corresponding to one of the following types: 1) dry mouth, 2) insomnia, 3) urinary hesitation/flow decrease, 4) constipation, 5) nausea, 6) decreased appetite, 7) feeling jittery, and 8) somnolence. Then patient i 's AE burden is $B_i = \sum_c \sum_g w_{cg} Y_{icg}$. Specification of the weights w_{cg} is subjective and should be elicited from subject matter experts. We define $w_{cg} = w_c w_g$ and set grade weights $w_g = g$. Higher type weights w_c may be given to more burdensome types of AEs if desired. As was noted in (Schweitzer et al., 2023), the AEs which led to study discontinuation included insomnia, nausea, and dry mouth. We assign these AEs weights which are 5 times higher than the others and thus $\mathbf{w}_c = (5, 5, 1, 1, 5, 1, 1, 1)$. Interestingly, this study suggested that the 2.5mg/75mg combination decreased the frequency of AEs overall, as well as the frequency of more burdensome AEs as compared to the 0mg/75mg combination. This non-monotonicity in the dose-toxicity relationship is captured in the simulations that follow.

We define Z_1 as OSA severity, where $Z_1 = 0$ corresponds to the mild/moderate subtype and $Z_1 = 1$ corresponds to the severe subtype. We define $f(\mathbf{d}, z_1)$ as the reduction in AHI_4 from baseline and $g(\mathbf{d}, z_1) = \log(B + 0.5)$ as the log-transformed AE burden score. Using efficacy and adverse event results from (Schweitzer et al., 2023), we fit flexible linear models on standardized doses to determine the parameters used in the data generating mechanisms for $f(\mathbf{d}, z_1)$ and $g(\mathbf{d}, z_1)$, whose functional forms are included in Table 1 (rows labeled ‘‘OSA’’) and which are plotted in Panel A of Figure 3 on the original dosage scale. The $f(\mathbf{d}, z_1)$ differ across the strata, where the parameter vector for $Z_1 = 0$ is $\beta_{Z_1=0} = (-1.38, -4.08, -0.48, -4.23, 2.45, -7.51, -1.56)$ and the parameter vector for $Z_1 = 1$ is $\beta_{Z_1=1} = (1.05, -11.28, -8.32, -17.02, 8.17, 2.34, 4.61)$. The $g(\mathbf{d}, z_1)$ is the same across strata and has parameter vector $\theta = (-0.59, 1.83, 2.26, -4.05, 1.79, 0.47, 2.91)$. As mentioned previously, under the personalized algorithm, we permit the tolerable toxicity thresholds to vary by strata. For the severe subtype, we set $g_1^\dagger = 2$, which equates to accepting an average AE burden score of about 7. This may include, for example, a single low-grade but high burden AE, or a couple moderate-grade but low burden AEs on average. For the mild/moderate subtype, we set $g_0^\dagger = 1.5$, which equates to accepting an average AE burden score of about 4. This may in-

clude, for example, a couple low-to-moderate-grade AEs of low burden, but would exclude higher burden AEs on average. The standard algorithm uses only a single value of the tolerable toxicity threshold, which we set equal to that of the mild/moderate subgroup, $g^\dagger = 1.5$.

Below we compare 12 designs using a maximum sample size of 100. The 12 designs are comprised of 6 personalized and 6 standard designs, where each uses a different combination of algorithm setting and stopping rule. The two settings differ in the number of patients assigned to each dose combination, where a larger number results in potentially fewer algorithm iterations, and a smaller number results in potentially more algorithm iterations. For the personalized algorithm, this is $r_k = 1$ and $r_k = 2$, and for the standard algorithm this is $r_k = 2$ and $r_k = 4$, respectively. We refer to these designs by their algorithm type and the degree of replication: $P1/P2$ for the personalized designs, and $S2/S4$ for the standard designs. The three stopping rules investigated permit early stopping at roughly 40, 60, or 80 patients, and are denoted by $n_{STOP} = \{40, 60, 80\}$. Recall that we permit early stopping in stratum k when $\max_{\tilde{\mathbf{d}} \in \mathbb{D}} \alpha_{cEI}(\tilde{\mathbf{d}}_k \mid \mathcal{D}) < \delta_k$ at least $(J + 1)$ times, which, for the dual-agent combination therapy being investigated, equates to 3 times. Within each design, we use the same value of δ_k for each stratum, and so $\delta_k = \delta$. The values of δ are calibrated such that each design achieves an expected sample size which is approximately the corresponding value of n_{STOP} . For $P1/P2$, $\delta = (0.1, 0.08, 0.065)/(0.137, 0.087, 0.07)$, and for $S2/S4$, $\delta = (0.077, 0.06, 0.05)/(0.1, 0.073, 0.055)$. The personalized algorithm permits stratum-specific early stopping, where the remaining budget is allocated to the other stratum where dose-finding may continue in the event of one of the strata stopping early. Finally, as there are no serious adverse events expected, we permit the modified dose combination region $\mathbb{D}_k^{(q)*}$ to expand at a quicker rate using $\rho_k = 0.5$. All other modeling and inferential details follow those previously described in the simulation study section. The performance of the designs is assessed and compared via the previously defined criteria which are estimated using 1,000 Monte Carlo replicates.

Under this scenario, we find that all designs yield expected sample sizes corresponding to their respective values of n_{STOP} (Panel B of Figure 3). The personalized algorithms converge to the $\mathbf{d}_{opt,k}$, with the optimization being more efficient in stratum $Z_1 = 0$ which has the larger ses_f

(Panel D of Figure 3). The standard algorithms are more efficient in converging to $\mathbf{d}_{opt,0}$, but fail to converge to $\mathbf{d}_{opt,1}$. Similar results hold for estimation of $f_{opt,k}$, where the personalized algorithms can handle the heterogeneity across strata whereas the standard algorithms cannot. We note that the personalized designs generally lead to a slightly larger number of participants receiving toxic doses (Panel C of Figure 3), but this results from these designs exploring more doses on average. For example, designs $P1/P2$ under $n_{STOP} = 40$ are expected to evaluate 11/9 unique doses whereas designs $S2/S4$ under $n_{STOP} = 40$ are expected to evaluate 7/6 unique doses (results not shown). We find that a lower degree of replication may lead to an increased probability of incorrectly determining that no feasible doses exist (i.e., $P1/S2$ vs $P2/S4$ in Panel F of Figure 3), and that for the personalized algorithm, this is more extreme in stratum $Z_1 = 0$ which has the more stringent toxicity threshold $g_0^\dagger = 1.5$. Note that the standard algorithm yields a single decision only, so this probability is fixed across strata. Given the goal of the trial is to identify subtype-tailored dose combinations, the standard designs would be unusable in practice. Furthermore, we exclude design $P1$ from consideration as it yields a substantial increase in the probability of declaring no feasible doses as compared to $P2$. Based upon the simulated scenario, we would recommend $P2$ with either $n_{STOP} = 60$ or $n_{STOP} = 80$ given their improvements over $P2$ with $n_{STOP} = 40$. Design $P2$ with $n_{STOP} = 60$ is expected to evaluate 10 unique doses in 64 patients with 14 receiving toxic doses on average, whereas design $P2$ with $n_{STOP} = 80$ is expected to evaluate 11 unique doses in 80 patients with 16 receiving toxic doses on average. The study investigator could make a final decision by performing a cost-benefit analysis using these estimates.

6 Discussion

In this work, we generalized the methods proposed in Willard et al. (2023) to the setting of higher-grade continuous toxicities under no monotonicity assumptions. We showed how these toxicities could be incorporated into the search strategy employed by the Bayesian optimization methods, as well as proposed a dose-escalation scheme to collect the initial data. A personalized approach is shown to be beneficial when response heterogeneity exists in at least one of the efficacy and toxicity surfaces. Additionally, the personalized approach permits tolerable levels of toxicity to

be defined with respect to individual strata, providing an additional level of tailoring which is not possible when utilizing the standard approach.

The proposed work is not without limitations. Firstly, all simulations were performed using a single binary covariate under the setting of dual-agent dose combinations only. Under the personalized approach, the use of additional categorical variables or dosing agents is straightforward, though would require larger sample sizes. Extension to continuous covariates remains as future work. While conceptually straightforward under the proposed approach, the dangers and consequences of inadvertently extrapolating into regions of covariate combinations never before seen in the trial would need to be considered and assessed. Secondly, future research should investigate the impact of a wider range of dose escalation schemes on overall algorithm performance than those that are featured here. As this may be applicable to a variety of constrained Bayesian optimization problems outside of dose-finding, this is a particularly interesting research direction. Finally, we assumed conditional independence between the efficacy and toxicity surfaces. This assumption could be relaxed by jointly modeling the efficacy and toxicity responses using a multivariate GP. The cEI acquisition function would need to be updated to incorporate the correlation between the two responses. We leave this as a direction for future work.

Changes to the GP modeling and acquisition function may help improve performance of the algorithms. Stationary, anisotropic squared exponential kernels were used but could be replaced by *non-stationary* kernels which include dose-covariate interaction terms. These would permit the correlation between two dose combinations to depend on the actual dosage levels and strata in which they lie, rather than solely on their distance from one another in the input space. Doing so, however, may greatly increase the dimensionality of the hyperparameter space, potentially leading to the same estimation challenges the proposed methods sought to avoid. Additionally, an empirical Bayes approach was adopted toward the GP hyperparameters, where initial values of the hyperparameters were used until the maximum likelihood estimation routines converged. While convenient and practical, proceeding in a fully Bayesian manner by placing priors on all hyperparameters may improve estimation at the earlier stages of optimization. However, this comes at the

increased computational cost of posterior sampling, which could be prohibitive depending on the number of scenarios of interest and the expected number of algorithm iterations, each of which requires refitting the GP models. Finally, the cEI acquisition function utilizes a point estimate of the current best observation, $f_k^* = \min_{\tilde{\mathbf{d}} \in \mathbb{A}_k} \mu_f(\tilde{\mathbf{d}}_k)$, which ignores the uncertainty around this quantity. Proceeding in a fully Bayesian manner by integrating over its posterior distribution may yield efficiency gains. Two different acquisition functions adopt this approach (Gramacy et al., 2016; Letham et al., 2019), but are not available analytically and require Monte Carlo for evaluation. While utilization of these acquisition functions would greatly increase the computational burden of the proposed dose-finding algorithm, they represent an exciting direction for future work.

Data Availability

No new data were created or analyzed in this study. The R scripts used for the simulations and graphics can be found on a public GitHub repository at https://github.com/jjwillard/bayesopt_obdc.

Acknowledgments

The authors would like to thank Dr. John Kimoff for his valued input regarding the OSA application component of this manuscript. JW acknowledges the support of a doctoral training scholarship from the Fonds de recherche du Québec - Nature et technologies (FRQNT). SG acknowledges the support by a Discovery Grant from the Natural Sciences and Engineering Research Council of Canada (NSERC), a Chercheurs-boursiers (Junior 1) award from the Fonds de recherche du Québec - Santé (FRQS), and support from the Canadian Statistical Sciences Institute. EEMM acknowledges support from a Discovery Grant from NSERC. EEMM is a Canada Research Chair (Tier 1) in Statistical Methods for Precision Medicine and acknowledges the support of a chercheur de mérite career award from the FRQS. This research was enabled in part by support provided by Calcul Québec and the Digital Research Alliance of Canada.

Disclosures

The authors report there are no competing interests to declare.

References

- Aishah, A., Loffler, K. A., Toson, B., Mukherjee, S., Adams, R. J., Altree, T. J., Ainge-Allen, H. W., Yee, B. J., Grunstein, R. R., Carberry, J. C., et al. (2023). One Month Dosing of Atomoxetine Plus Oxybutynin in Obstructive Sleep Apnea: a Randomized, Placebo-Controlled Trial. *Annals of the American Thoracic Society*, 20(4):584–595.
- Babb, J., Rogatko, A., and Zacks, S. (1998). Cancer Phase I Clinical Trials: Efficient Dose Escalation with Overdose Control. *Statistics in Medicine*, 17(10):1103–1120.
- Babb, J. S. and Rogatko, A. (2001). Patient Specific Dosing in a Cancer Phase I Clinical Trial. *Statistics in Medicine*, 20(14):2079–2090.
- Benjafield, A. V., Ayas, N. T., Eastwood, P. R., Heinzer, R., Ip, M. S., Morrell, M. J., Nunez, C. M., Patel, S. R., Penzel, T., Pépin, J.-L., et al. (2019). Estimation of the Global Prevalence and Burden of Obstructive Sleep Apnoea: a Literature-Based Analysis. *The Lancet Respiratory Medicine*, 7(8):687–698.
- Berry, S. M., Carlin, B. P., Lee, J. J., and Muller, P. (2010). *Bayesian Adaptive Methods for Clinical Trials*. CRC Press, Boca Raton, FL.
- Binois, M. and Gramacy, R. B. (2021). hetgp: Heteroskedastic Gaussian Process Modeling and Sequential Design in R. *Journal of Statistical Software*, 98(13):1–44.
- Chen, Z., Krailo, M. D., Azen, S. P., and Tighiouart, M. (2010). A Novel Toxicity Scoring System Treating Toxicity Response as a Quasi-Continuous Variable in Phase I Clinical Trials. *Contemporary Clinical Trials*, 31(5):473–482.
- Farewell, V. T., Tom, B. D. M., and Royston, P. (2004). The Impact of Dichotomization on the Efficiency of Testing for an Interaction Effect in Exponential Family Models. *Journal of the American Statistical Association*, 99(467):822–831.
- Gardner, J. R., Kusner, M. J., Xu, Z. E., Weinberger, K. Q., and Cunningham, J. P. (2014). Bayesian Optimization with Inequality Constraints. In *Proceedings of the 31st International Conference on Machine Learning*. 32:937–945.

- Garnett, R. (2023). *Bayesian Optimization*. Cambridge University Press, Cambridge, UK.
- Gelbart, M. A., Snoek, J., and Adams, R. P. (2014). Bayesian Optimization with Unknown Constraints. *arXiv preprint arXiv:1403.5607*.
- Golchi, S., Bingham, D. R., Chipman, H., and Campbell, D. A. (2015). Monotone Emulation of Computer Experiments. *SIAM/ASA Journal on Uncertainty Quantification*, 3(1):370–392.
- Gramacy, R. B. (2020). *Surrogates: Gaussian Process Modeling, Design and Optimization for the Applied Sciences*. Chapman Hall/CRC, Boca Raton, FL.
- Gramacy, R. B., Gray, G. A., Le Digabel, S., Lee, H. K., Ranjan, P., Wells, G., and Wild, S. M. (2016). Modeling an Augmented Lagrangian for Blackbox Constrained Optimization. *Technometrics*, 58(1):1–11.
- Guo, B. and Zang, Y. (2022). A Bayesian Phase I/II Biomarker-Based Design for Identifying Subgroup-Specific Optimal Dose for Immunotherapy. *Statistical Methods in Medical Research*, 31(6):1104–1119.
- Houede, N., Thall, P. F., Nguyen, H., Paoletti, X., and Kramar, A. (2010). Utility-Based Optimization of Combination Therapy Using Ordinal Toxicity and Efficacy in Phase I/II Trials. *Biometrics*, 66(2):532–540.
- Huang, D., Allen, T. T., Notz, W. I., and Zeng, N. (2006). Global Optimization of Stochastic Black-Box Systems via Sequential Kriging Meta-Models. *Journal of Global Optimization*, 34:441–466.
- Jones, D. R., Schonlau, M., and Welch, W. J. (1998). Efficient Global Optimization of Expensive Black-Box Functions. *Journal of Global Optimization*, 13:455–492.
- Korn, E. L. (2004). Nontoxicity Endpoints in Phase I Trial Designs for Targeted, Non-Cytotoxic Agents. *Journal of the National Cancer Institute*, 96(13):977–978.
- Kushner, H. (1964). A New Method of Locating the Maximum Point of an Arbitrary Multipeak Curve in the Presence of Noise. *Journal of Basic Engineering*, 86(1):97–106.

- Le-Rademacher, J. G., Hillman, S., Storrick, E., Mahoney, M. R., Thall, P. F., Jatoi, A., and Mandrekar, S. J. (2020). Adverse Event Burden Score — a Versatile Summary Measure for Cancer Clinical Trials. *Cancers*, 12(11):3251.
- Le Tourneau, C., Lee, J. J., and Siu, L. L. (2009). Dose Escalation Methods in Phase I Cancer Clinical Trials. *JNCI: Journal of the National Cancer Institute*, 101(10):708–720.
- Lee, S., Hershman, D., Martin, P., Leonard, J., and Cheung, Y. (2012). Toxicity Burden Score: a Novel Approach to Summarize Multiple Toxic Effects. *Annals of Oncology*, 23(2):537–541.
- Letham, B., Karrer, B., Ottoni, G., and Bakshy, E. (2019). Constrained Bayesian Optimization with Noisy Experiments. *Bayesian Analysis*, 14(2):495–519.
- Li, D. H., Whitmore, J. B., Guo, W., and Ji, Y. (2017). Toxicity and Efficacy Probability Interval Design for Phase I Adoptive Cell Therapy Dose-Finding Clinical Trials. *Clinical Cancer Research*, 23(1):13–20.
- Lin, L. and Dunson, D. B. (2014). Bayesian Monotone Regression Using Gaussian Process Projection. *Biometrika*, 101(2):303–317.
- Mozgunov, P., Cro, S., Lingford-Hughes, A., Paterson, L. M., and Jaki, T. (2022). A Dose-Finding Design for Dual-Agent Trials with Patient-Specific Doses for One Agent with Application to an Opiate Detoxification Trial. *Pharmaceutical Statistics*, 21(2):476–495.
- Mozgunov, P. and Jaki, T. (2019a). A Flexible Design for Advanced Phase I/II Clinical Trials with Continuous Efficacy Endpoints. *Biometrical Journal*, 61(6):1477–1492.
- Mozgunov, P. and Jaki, T. (2019b). An Information Theoretic Phase I–II Design for Molecularly Targeted Agents that does not Require an Assumption of Monotonicity. *Journal of the Royal Statistical Society, Series C*, 68(2):347–367.
- O’Quigley, J., Pepe, M., and Fisher, L. (1990). Continual Reassessment Method: a Practical Design for Phase 1 Clinical Trials in Cancer. *Biometrics*, 46:33–48.
- R Core Team (2022). *R: A Language and Environment for Statistical Computing*. R Foundation for Statistical Computing, Vienna, Austria. <https://www.R-project.org/>.

- Rosenberg, R., Abaluck, B., and Thein, S. (2022). Combination of Atomoxetine with the Novel Antimuscarinic Aroxybutynin Improves Mild to Moderate OSA. *Journal of Clinical Sleep Medicine*, 18(12):2837–2844.
- Rotenberg, B. W., Murariu, D., and Pang, K. P. (2016). Trends in CPAP Adherence Over Twenty Years of Data Collection: a Flattened Curve. *Journal of Otolaryngology-Head & Neck Surgery*, 45(1):43.
- Royston, P., Altman, D. G., and Sauerbrei, W. (2006). Dichotomizing Continuous Predictors in Multiple Regression: a Bad Idea. *Statistics in Medicine*, 25(1):127–141.
- Schweitzer, P. K., Taranto-Montemurro, L., Ojile, J. M., Thein, S. G., Drake, C. L., Rosenberg, R., Corser, B., Abaluck, B., Sangal, R. B., and Maynard, J. (2023). The Combination of Aroxybutynin and Atomoxetine in the Treatment of Obstructive Sleep Apnea (MARIPOSA): a Randomized Controlled Trial. *American Journal of Respiratory and Critical Care Medicine*, 208(12):1316–1327.
- Sweeting, M. J. and Mander, A. P. (2012). Escalation Strategies for Combination Therapy Phase I Trials. *Pharmaceutical Statistics*, 11(3):258–266.
- Takahashi, A. and Suzuki, T. (2021a). Bayesian Optimization Design for Dose-Finding Based on Toxicity and Efficacy Outcomes in Phase I/II Clinical Trials. *Pharmaceutical Statistics*, 20(3):422–439.
- Takahashi, A. and Suzuki, T. (2021b). Bayesian Optimization for Estimating the Maximum Tolerated Dose in Phase I Clinical Trials. *Contemporary Clinical Trials Communications*, 21:100753.
- Thall, P. F. and Cook, J. D. (2004). Dose-Finding Based on Efficacy-Toxicity Trade-Offs. *Biometrics*, 60(3):684–693.
- Thomas, N., Sweeney, K., and Somayaji, V. (2014). Meta-Analysis of Clinical Dose-Response in a Large Drug Development Portfolio. *Statistics in Biopharmaceutical Research*, 6(4):302–317.
- Wason, J. M., Mander, A. P., and Eisen, T. G. (2011). Reducing Sample Sizes in Two-Stage Phase II Cancer Trials by Using Continuous Tumour Shrinkage End-Points. *European Journal*

of Cancer, 47(7):983–989.

Willard, J., Golchi, S., Moodie, E. E., Boulanger, B., and Carlin, B. P. (2023). Bayesian Optimization for Personalized Dose-Finding Trials with Combination Therapies. *arXiv preprint arXiv:2310.17334*. Accessed 2024-02-08.

Yuan, Y., Nguyen, H. Q., and Thall, P. F. (2016). *Bayesian Designs for Phase I-II Clinical Trials*. Chapman and Hall, Boca Raton, FL.

Zhilinskas, A. (1975). Single-Step Bayesian Search Method for an Extremum of Functions of a Single Variable. *Cybernetics and Systems Analysis*, 11(1):160–166.

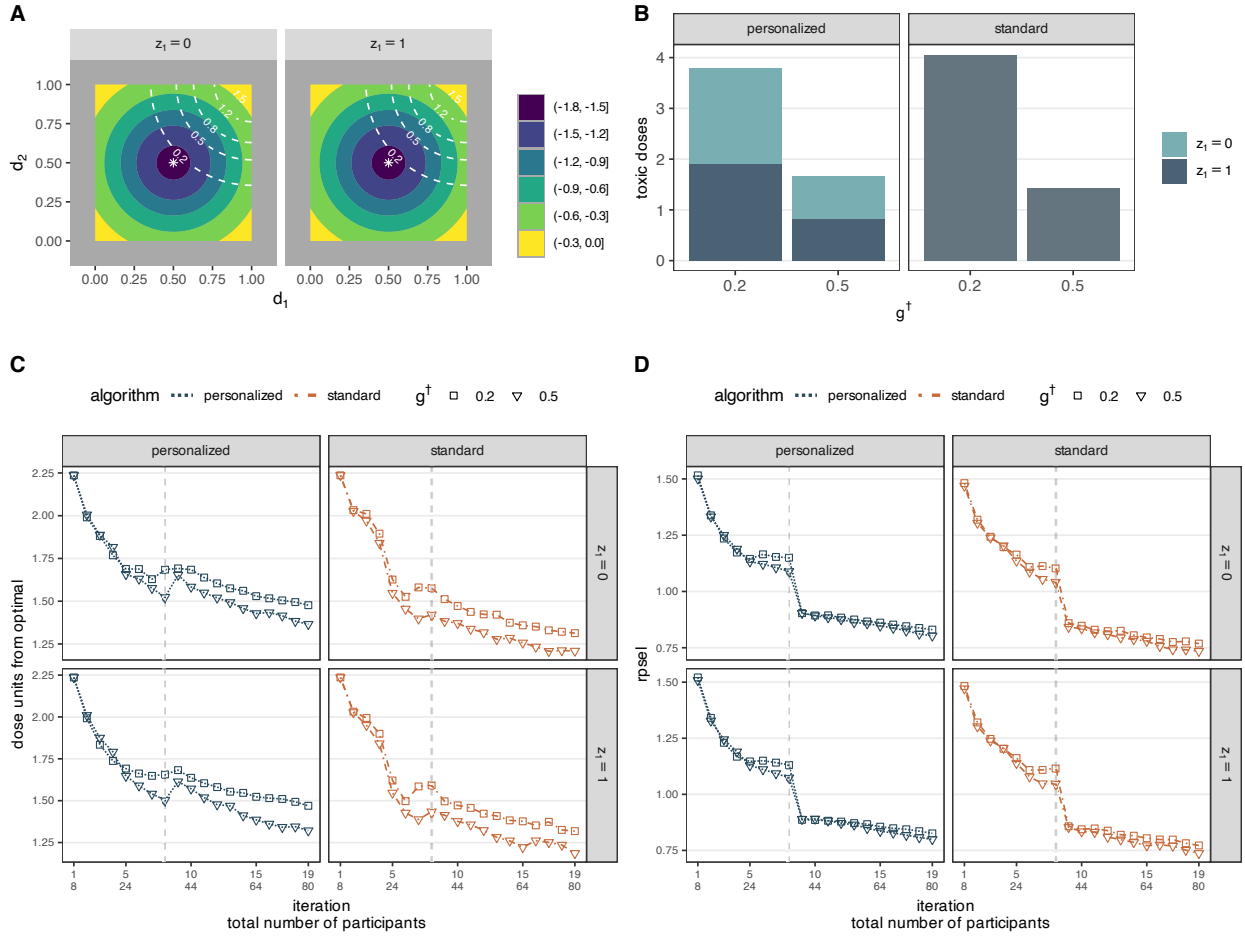


Figure 1: Scenario 1. A) Objective function, white stars denote $\mathbf{d}_{opt,k}$ and white dashed lines denote contours of toxicity function, B) expected number of truly toxic doses administered to participants as defined in (3), C) expected dose units from the optimal dose combination as defined in (4) by iteration, D) average RPSEL as defined in (5) by iteration. Vertical dashed lines in C and D represent iteration 8, after which the algorithm can search the entire dose combination space.

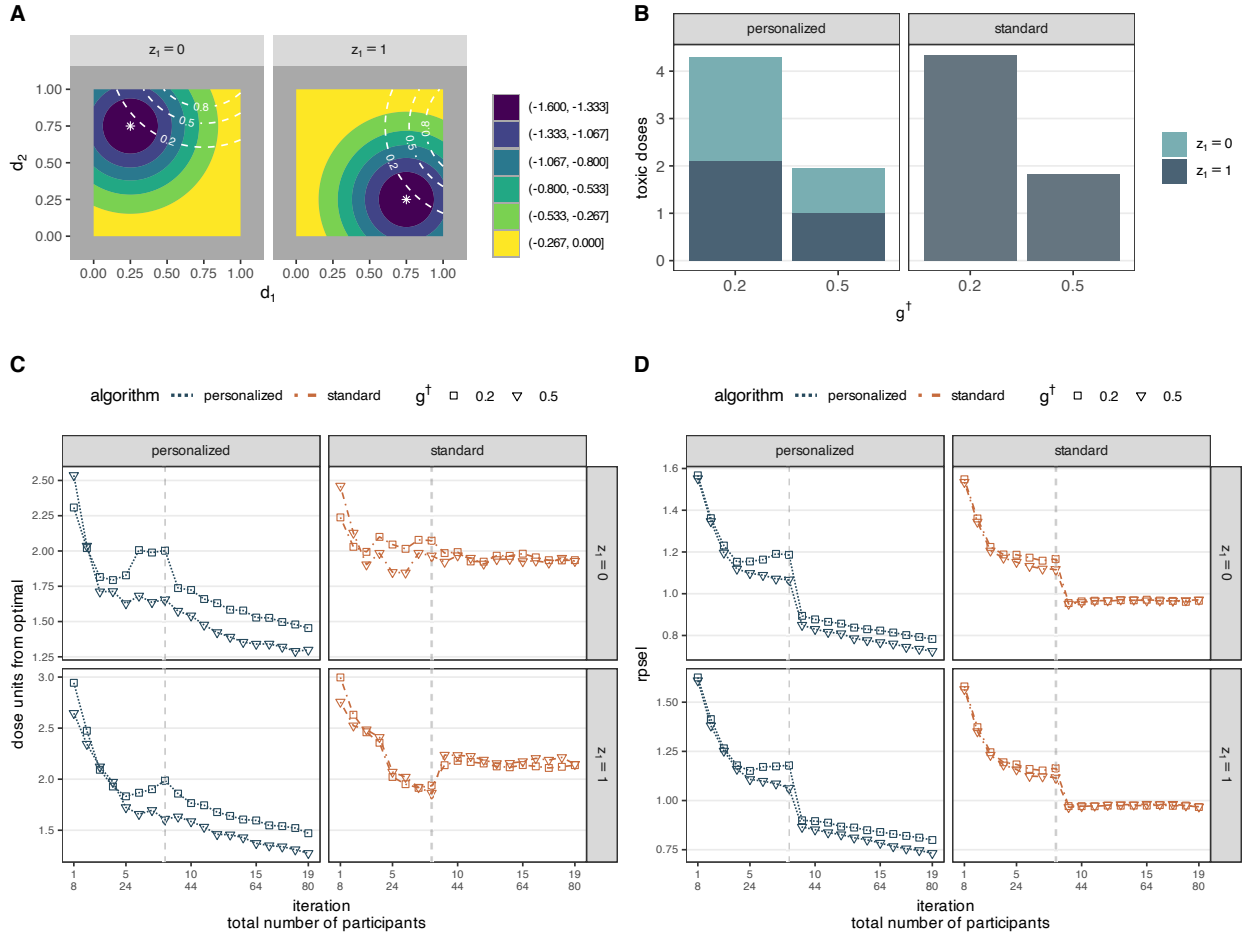


Figure 2: Scenario 2. A) Objective function, white stars denote $\mathbf{d}_{opt,k}$ and white dashed lines denote contours of toxicity function, B) expected number of truly toxic doses administered to participants as defined in (3), C) expected dose units from the optimal dose combination as defined in (4) by iteration, D) average RPSEL as defined in (5) by iteration. Vertical dashed lines in C and D represent iteration 8, after which the algorithm can search the entire dose combination space.

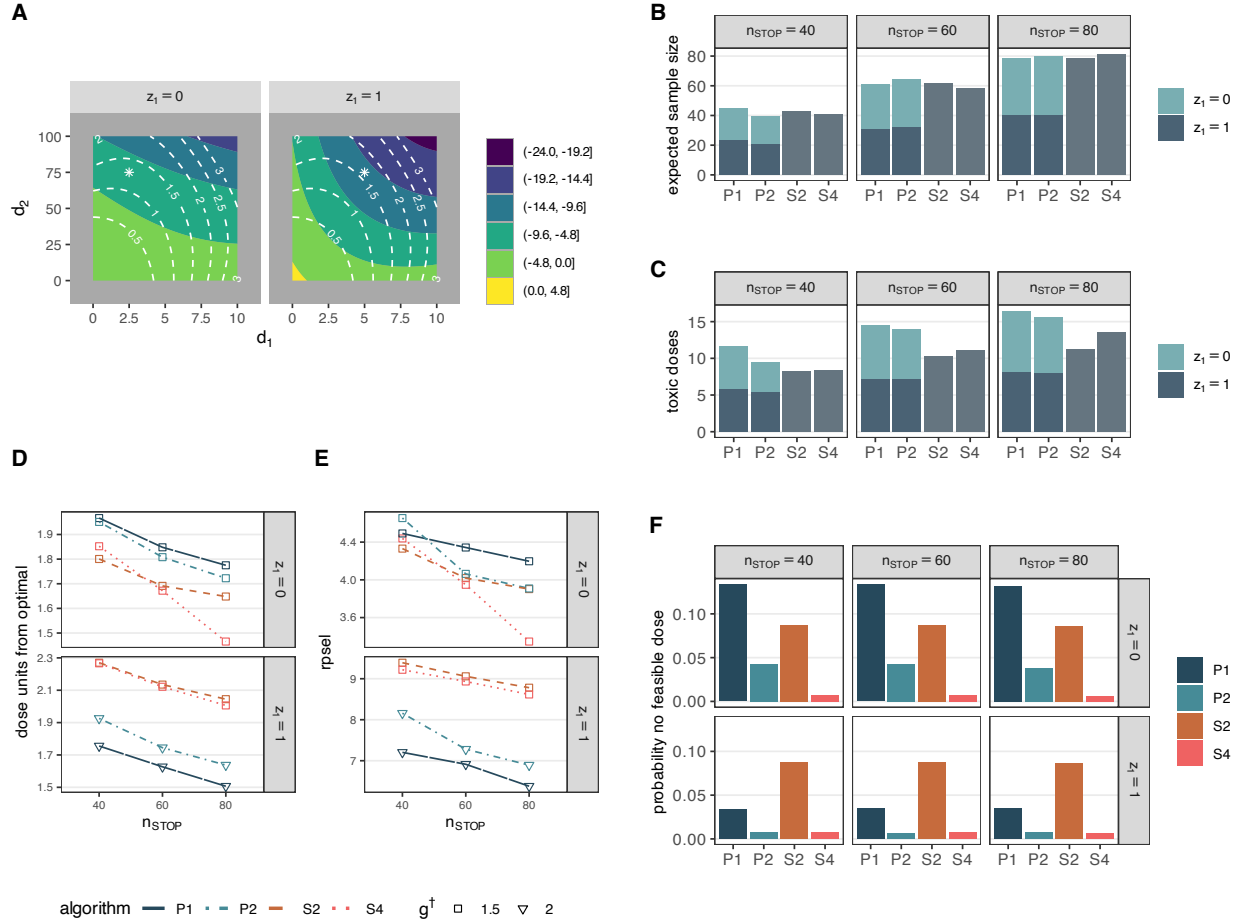


Figure 3: A) Objective function, white stars denote $\mathbf{d}_{opt,k}$, white dashed lines denote contours of toxicity function, B) expected sample size, C) expected number of truly toxic doses administered to participants as defined in (3), D) expected dose units from the optimal dose combination as defined in (4) by iteration, E) average RPSEL as defined in (5) by iteration, and F) probability of incorrectly stopping for toxicity and declaring no feasible doses. For OSA subtype, $Z_1 = 0$ denotes mild/moderate and $Z_1 = 1$ denotes severe.

Table 1: Simulation scenarios considered. The data generating mechanism for each scenario is $y_f = f(\mathbf{d}, z_1) + \epsilon_f$ and $y_g = g(\mathbf{d}, z_1) + \epsilon_g$ where $\epsilon_f \sim N(0, \sigma_{y_f}^2)$ and $\epsilon_g \sim N(0, \sigma_{y_g}^2)$. The table columns contain the location of the optimal dose combination (\mathbf{d}_{opt}), the value of the efficacy and toxicity functions at \mathbf{d}_{opt} (f_{opt}/g_{opt}), and the standardized effect sizes (ses_f/ses_g).

	$f(\mathbf{d}, z_1)$	$g(\mathbf{d}, z_1)$	σ_{y_f}	σ_{y_g}	z_1	\mathbf{d}_{opt}	f_{opt}	g_{opt}	ses_f	ses_g
Simulation Study	1) $-\mathbb{1}\{z_1 = 0\} \times h(\boldsymbol{\mu}_1) -$	$\mathbb{1}\{z_1 = 0\} \times h(\boldsymbol{\mu}_2) +$	1.59	0.13	0	(0.5, 0.5)	-1.59	0.13	1	1
	$\mathbb{1}\{z_1 = 1\} \times h(\boldsymbol{\mu}_1)$	$\mathbb{1}\{z_1 = 1\} \times h(\boldsymbol{\mu}_2)$			1	(0.5, 0.5)	-1.59	0.13	1	1
	2) $-\mathbb{1}\{z_1 = 0\} \times h(\boldsymbol{\mu}_3) -$	$\mathbb{1}\{z_1 = 0\} \times h(\boldsymbol{\mu}_5) +$	1.59	0.13	0	(0.25, 0.75)	-1.59	0.13	1	1
	$\mathbb{1}\{z_1 = 1\} \times h(\boldsymbol{\mu}_4)$	$\mathbb{1}\{z_1 = 1\} \times h(\boldsymbol{\mu}_6)$			1	(0.75, 0.25)	-1.59	0.13	1	1
OSA	1) $\beta_{z_1,0} + \beta_{z_1,1}d_1 + \beta_{z_1,2}d_2 +$	$\theta_0 + \theta_1d_1 + \theta_2d_2 +$	7.68	1.29	0	(2.5, 75)	-7.68	1.29	1	1
	$\beta_{z_1,3}d_1d_2 + \beta_{z_1,4}d_1^2 +$	$\theta_3d_1d_2 + \theta_4d_1^2 +$			1	(5, 75)	-13.20	1.63	1.72	1.26
	$\beta_{z_1,5}d_2^2 + \beta_{z_1,6}d_1^2d_2^2$	$\theta_5d_2^2 + \theta_6d_1^2d_2^2$								